

Supplementary Information

An all superantiwetting surface in water-oil-air systems

Lu Tie,^{ac} Jing Li,^{*a} Zhiguang Guo,^{*ab} Yongmin Liang^{ad} and Weimin Liu^{*a}

^a State Key Laboratory of Solid Lubrication, Lanzhou Institute of Chemical Physics, Chinese Academy of Sciences, Lanzhou 730000, People's Republic of China

^b Ministry of Education Key Laboratory for the Green Preparation and Application of Functional Materials, Hubei University, Wuhan 430062, People's Republic of China

^c University of Chinese Academy of Sciences, Beijing 100049, People's Republic of China

^d State Key Laboratory of Applied Organic Chemistry, Lanzhou University, Lanzhou 730000, People's Republic of China

*E-mail: jli@licp.cas.cn (J. Li); zguo@licp.cas.cn (Z. Guo); wmliu@licp.cas.cn (W. Liu).

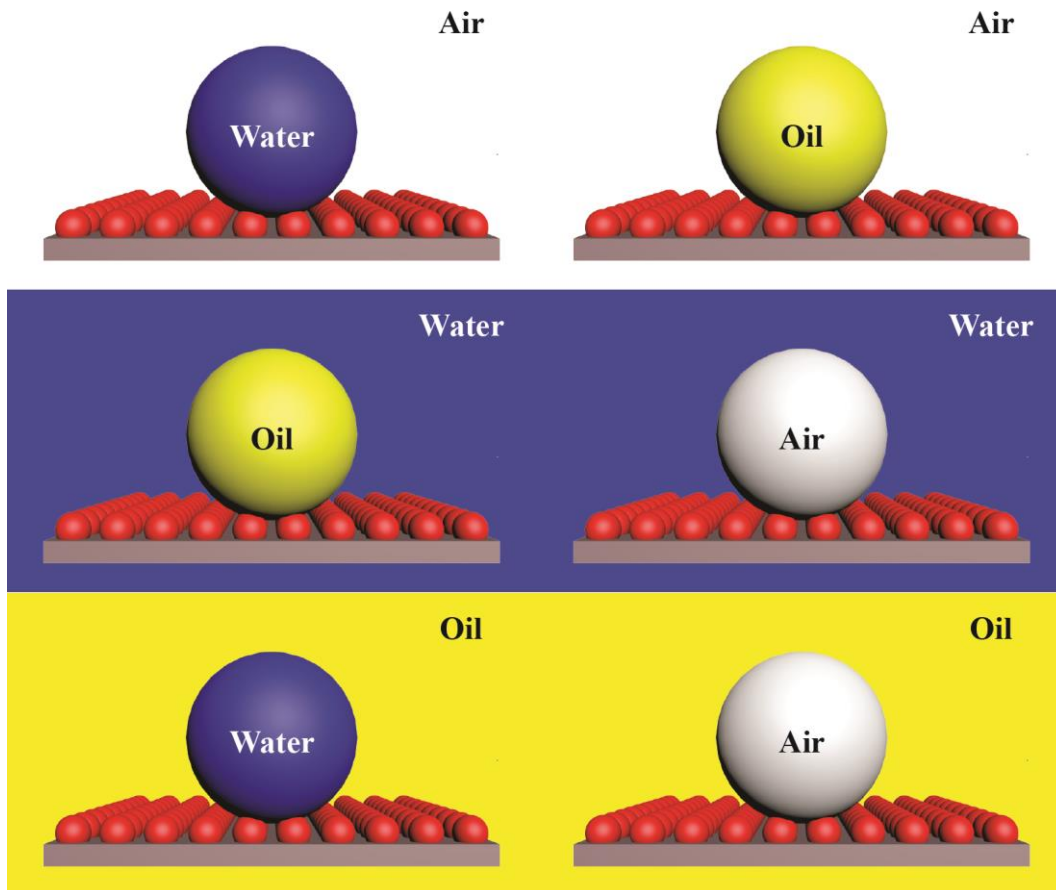


Fig. S1 Schematic illustration of all superantiwetting surfaces.

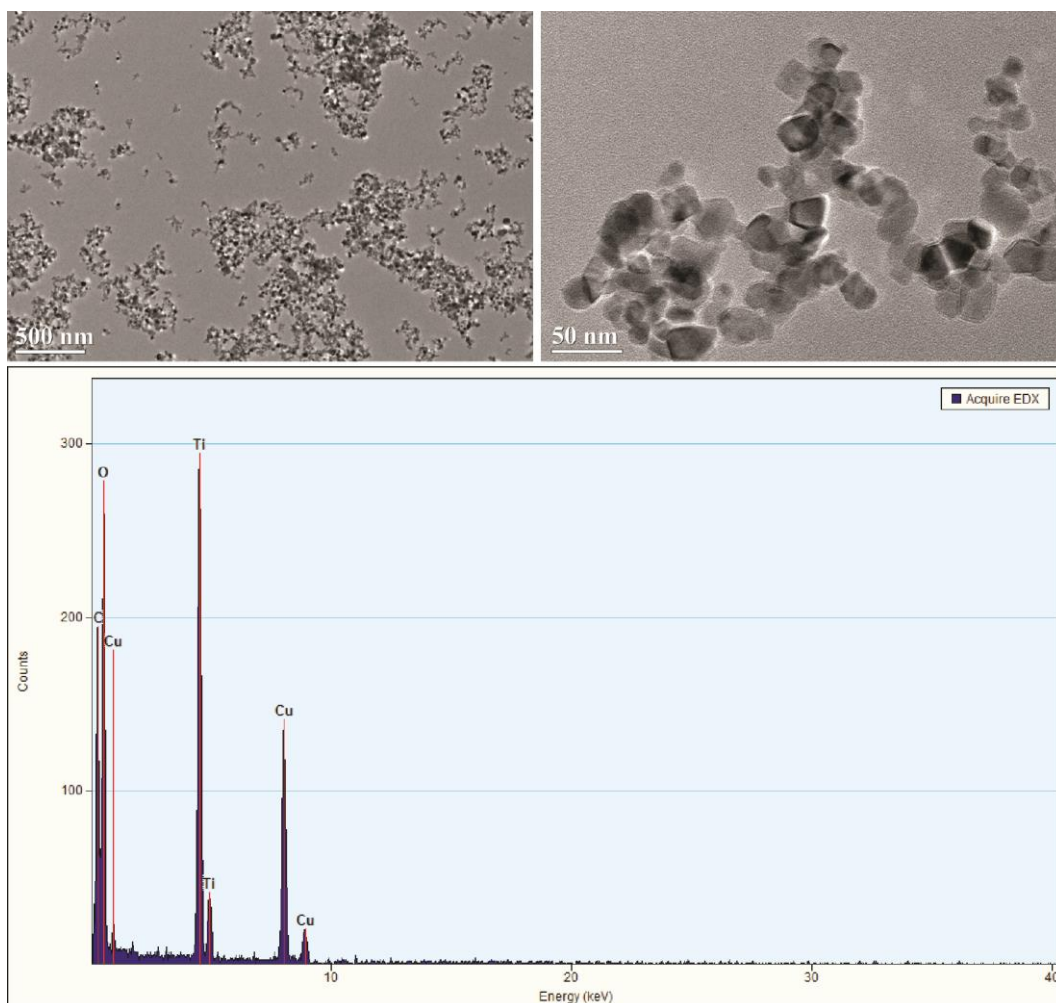


Fig. S2 TEM images and EDS spectrum of TiO_2 nanoparticles.

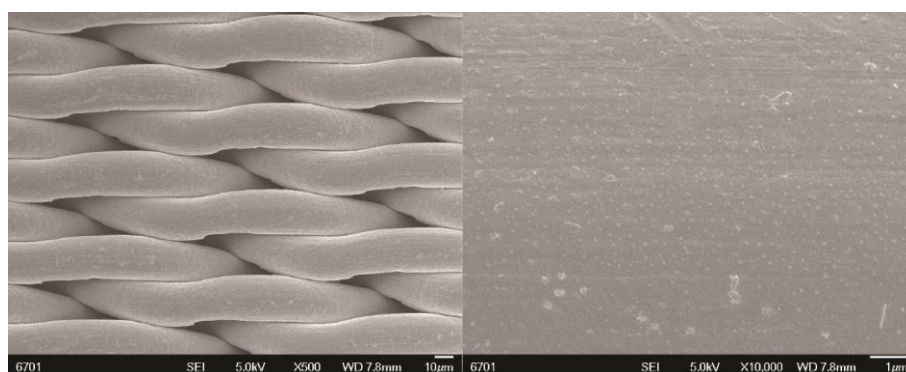


Fig. S3 SEM images of original SSM.

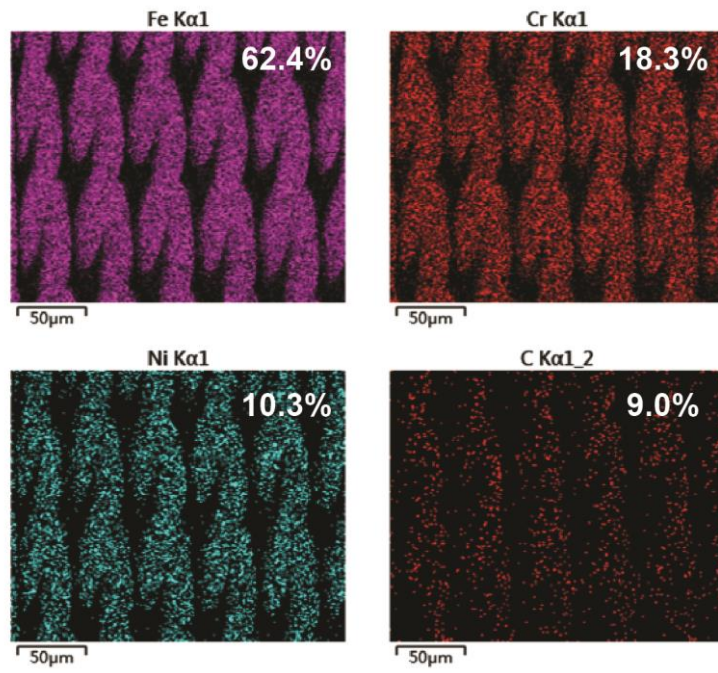


Fig. S4 Element distribution maps of original SSM.

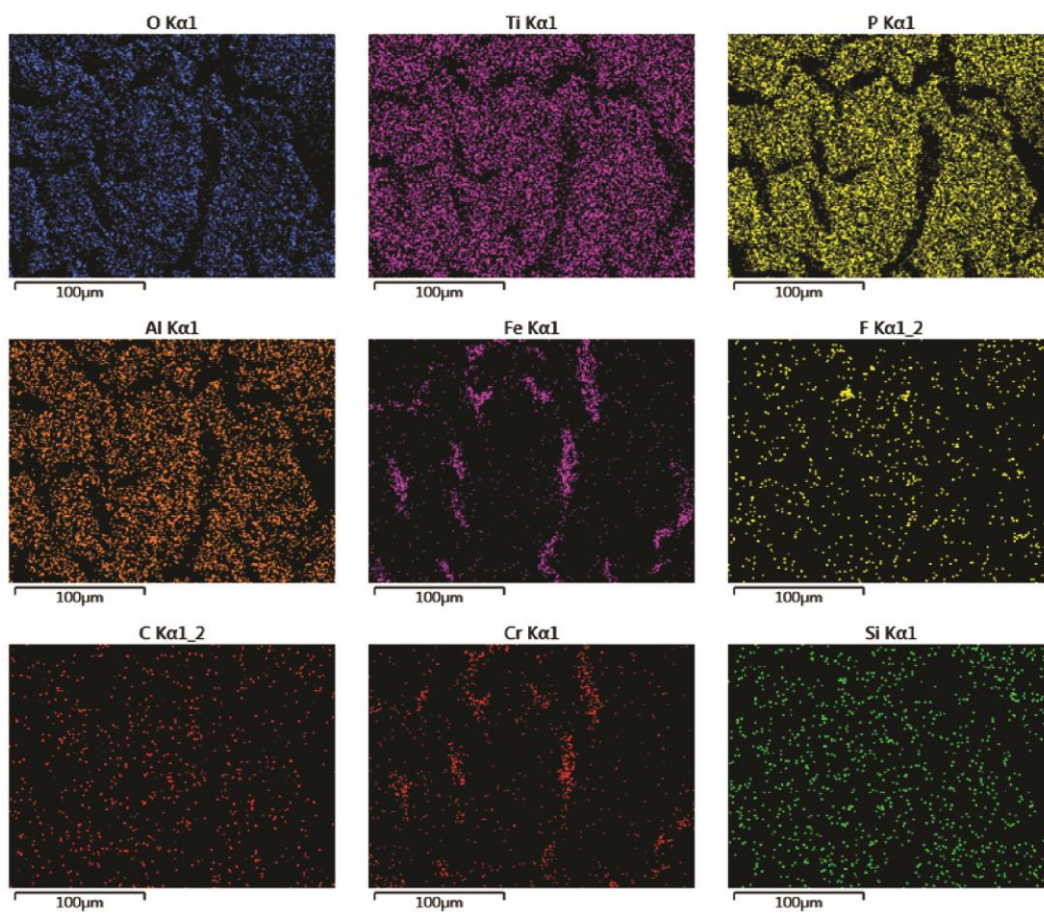


Fig. S5 Element distribution maps of the TiO₂-AP-FOTS coated SSM.

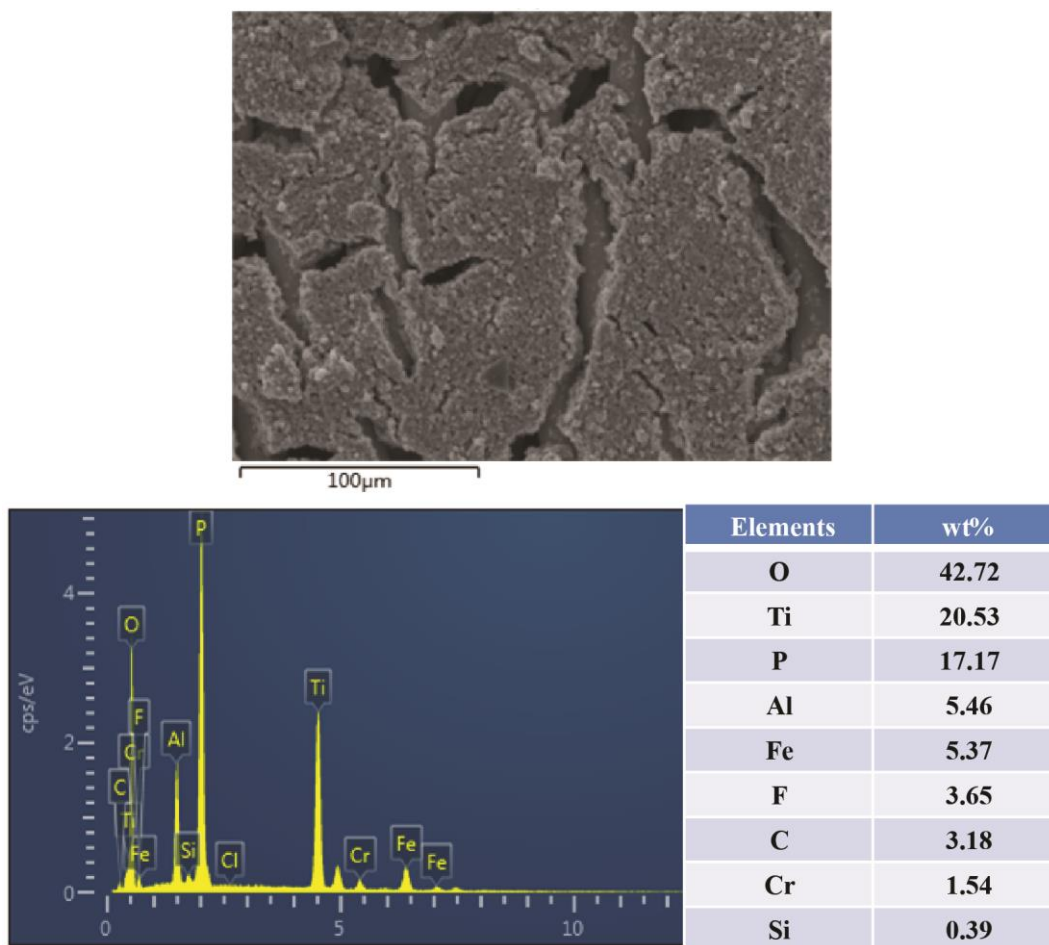


Fig. S6 SEM image and EDS spectrum of the TiO₂-AP-FOTS coated SSM.

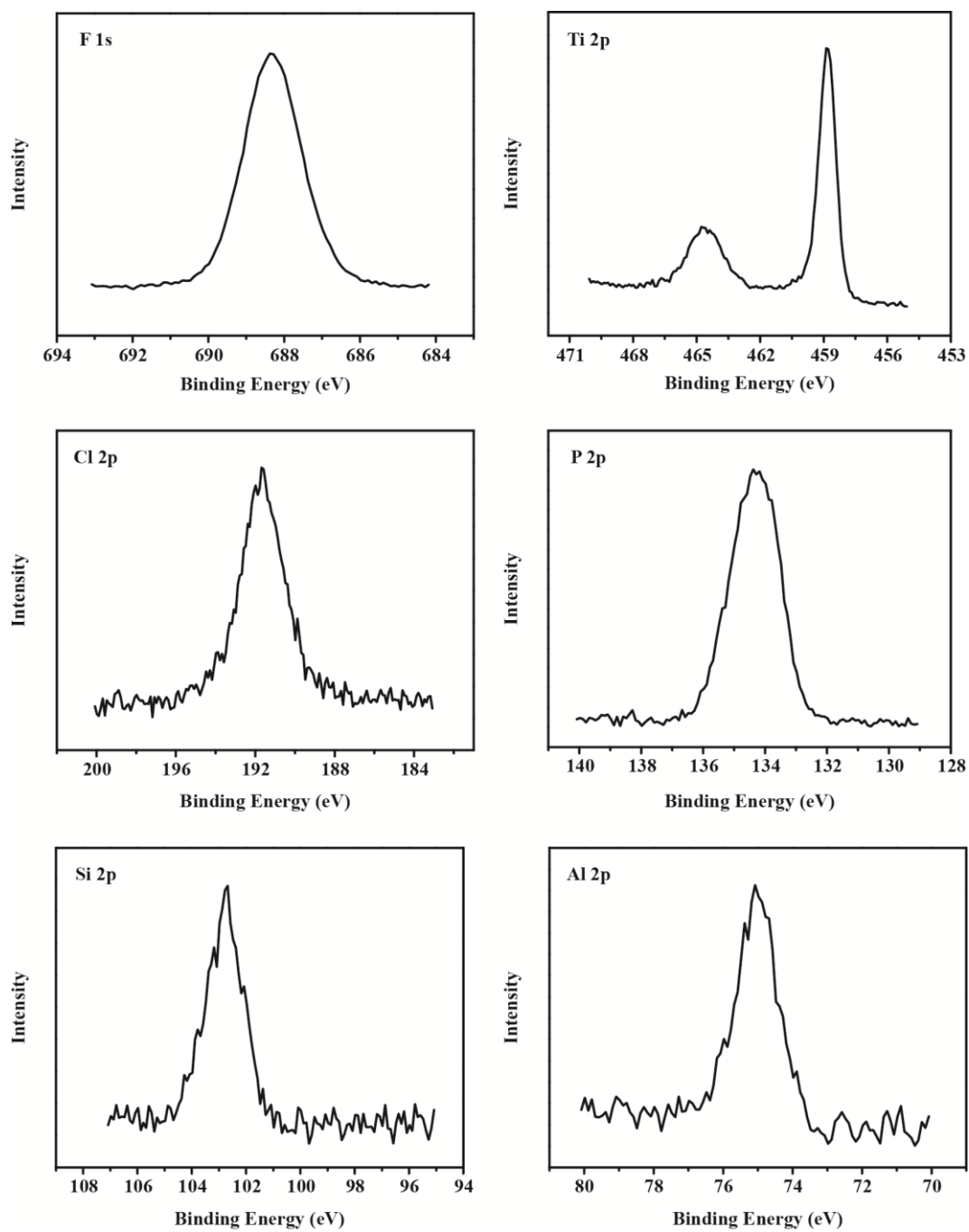


Fig. S7 XPS spectra of the TiO₂-AP-FOTS coated SSM.

Water in Air



Oil in Air



Oil in Water



Bubble in Water



Water in Oil



Bubble in Oil



Fig. S8 Photographs of the sliding processes for water in air, hexadecane in air, 1,2-dichloroethane under water, air bubble under water, water under hexane, and air bubble under hexane on the surface of the TiO₂-AP-FOTS coated SSM.

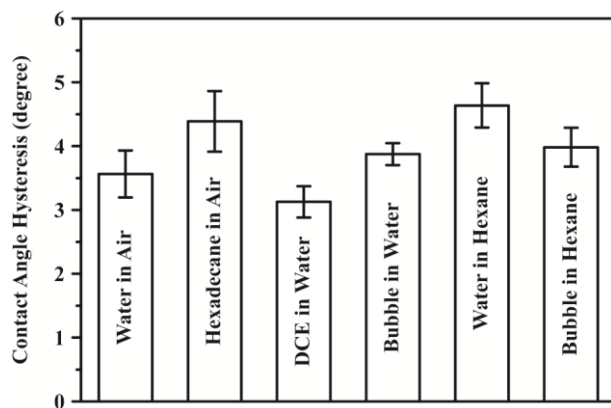


Fig. S9 Contact angle hysteresis of the TiO₂-AP-FOTS coated SSM for water in air, hexadecane in air, 1,2-dichloroethane under water, air bubble under water, water under hexane, and air bubble under hexane.

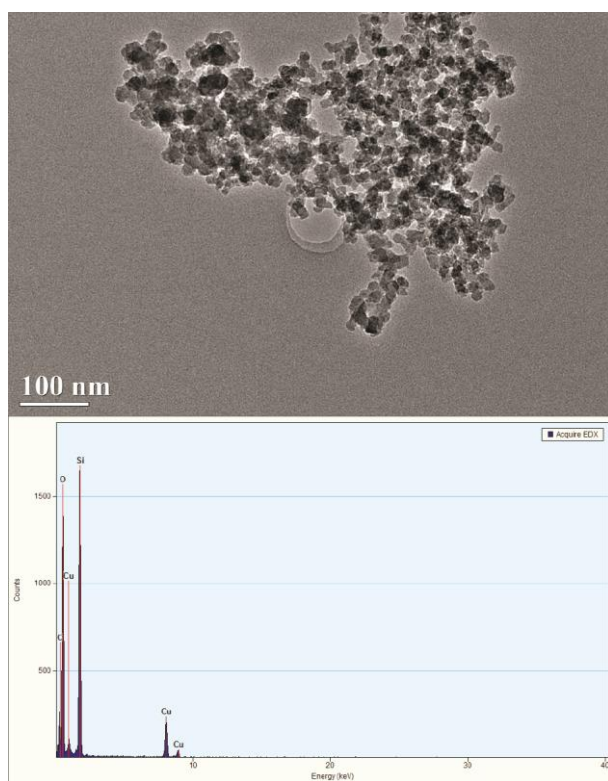


Fig. S10 TEM image and EDS spectrum of SiO₂ nanoparticles.

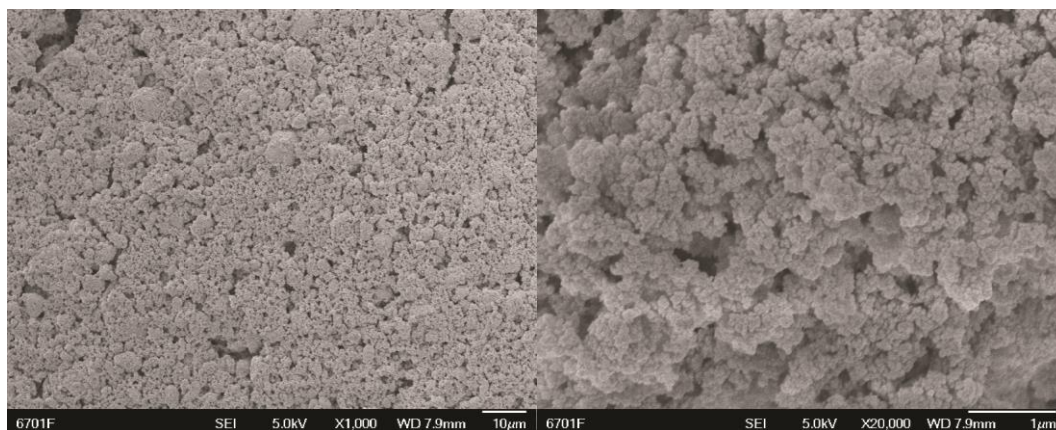


Fig. S11 SEM images of the SiO₂-AP-FOTS coated SSM.

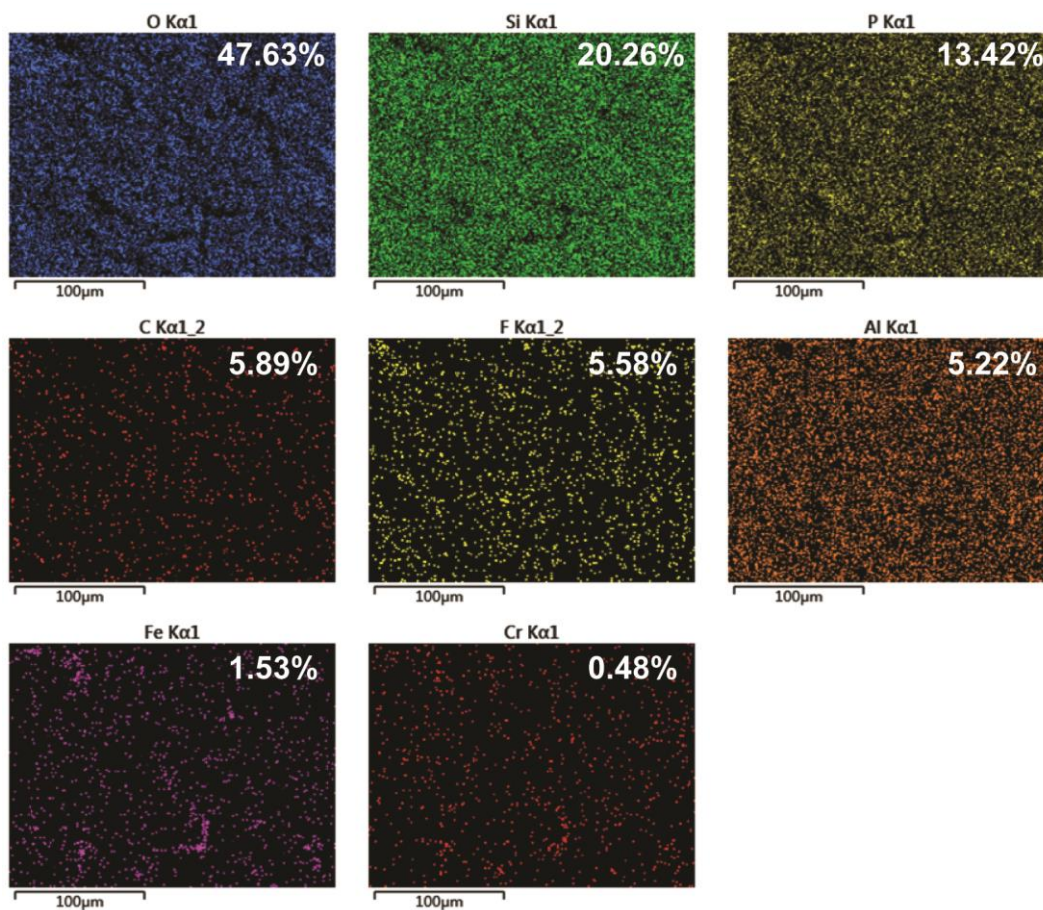


Fig. S12 Element distribution maps of the SiO₂-AP-FOTS coated SSM.

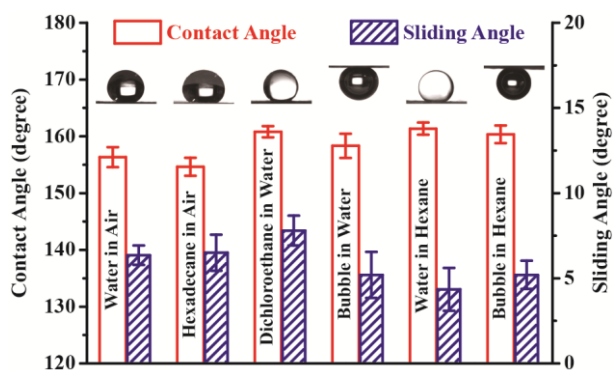


Fig. S13 Contact angles and sliding angles of the SiO₂-AP-FOTS coated SSM for water in air, hexadecane in air, 1,2-dichloroethane under water, air bubble under water, water under hexane, and air bubble under hexane.

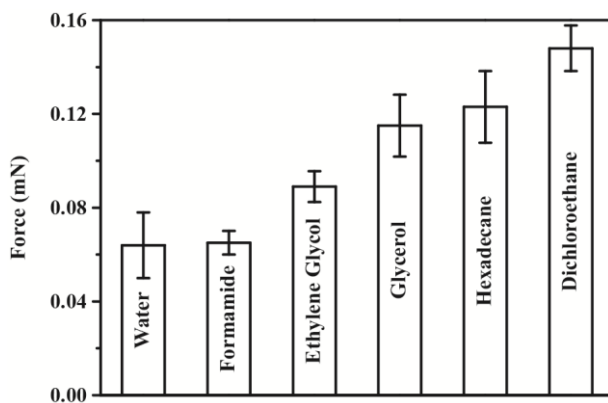


Fig. S14 Adhesive forces of water and oils deposited on the surface of the TiO₂-AP-FOTS coated SSM.

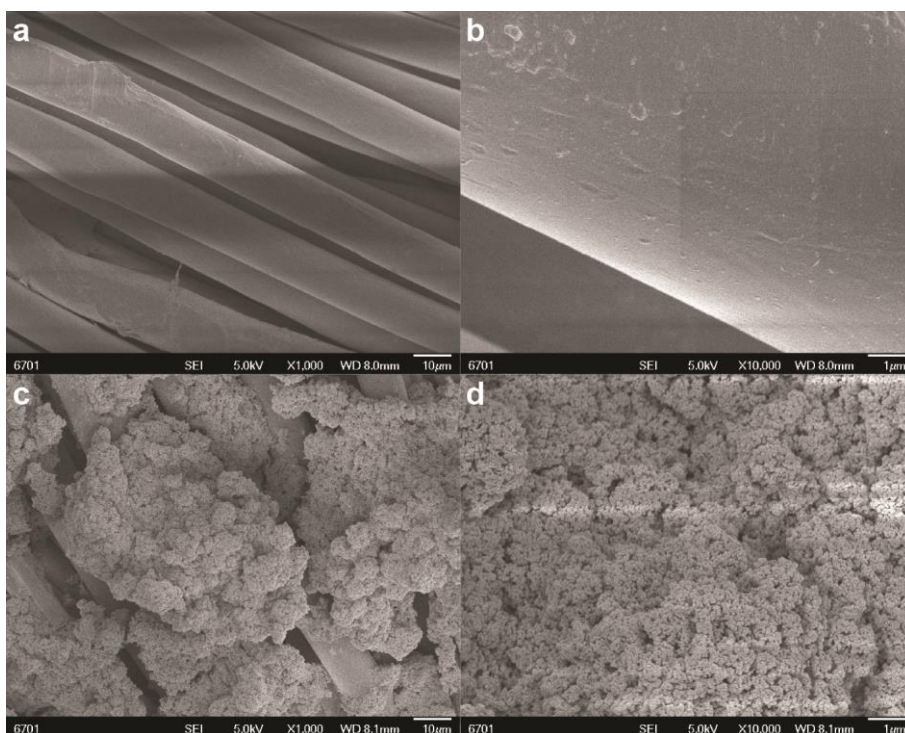


Fig. S15 SEM images of (a, b) original and (c, d) TiO₂-AP-FOTS coated fabrics.

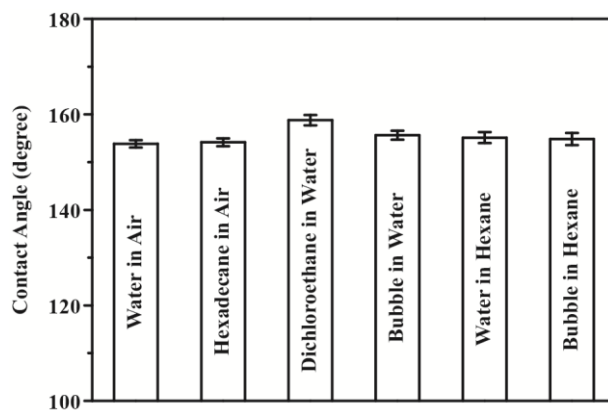


Fig. S16 Contact angles of the TiO₂-AP-FOTS coated fabric for water in air, hexadecane in air, 1,2-dichloroethane under water, air bubble under water, water under hexane, and air bubble under hexane.

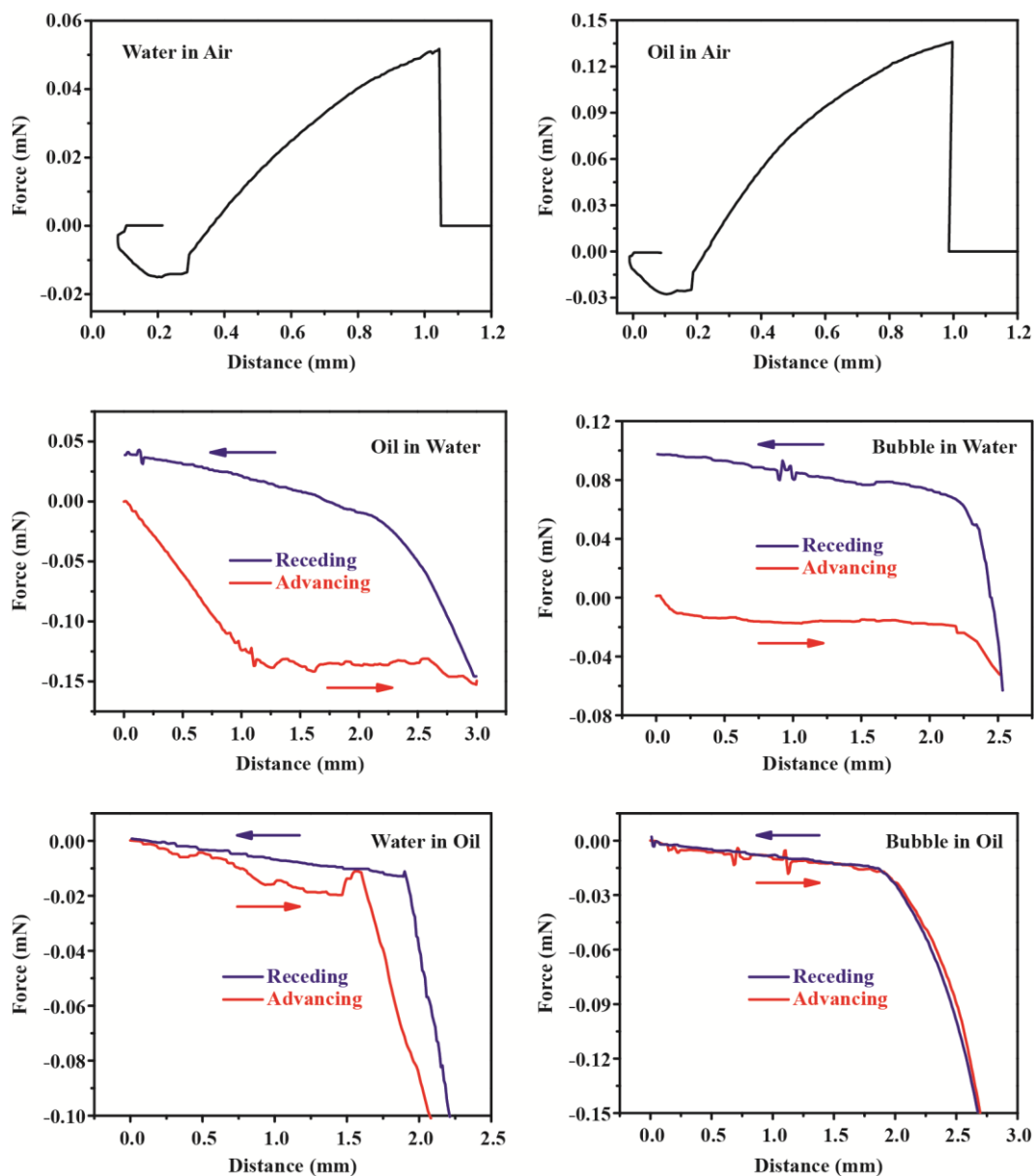


Fig. S17 Adhesion measurements of the TiO₂-AP-FOTS coated fabric: water in air, hexadecane in air, 1,2-dichloroethane under water, air bubble under water, water under hexane, and air bubble under hexane.

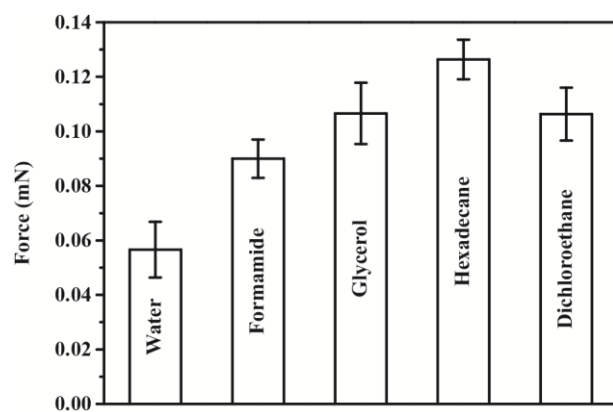


Fig. S18 Adhesive forces of water and oils deposited on the surface of the TiO₂-AP-FOTS coated fabric.

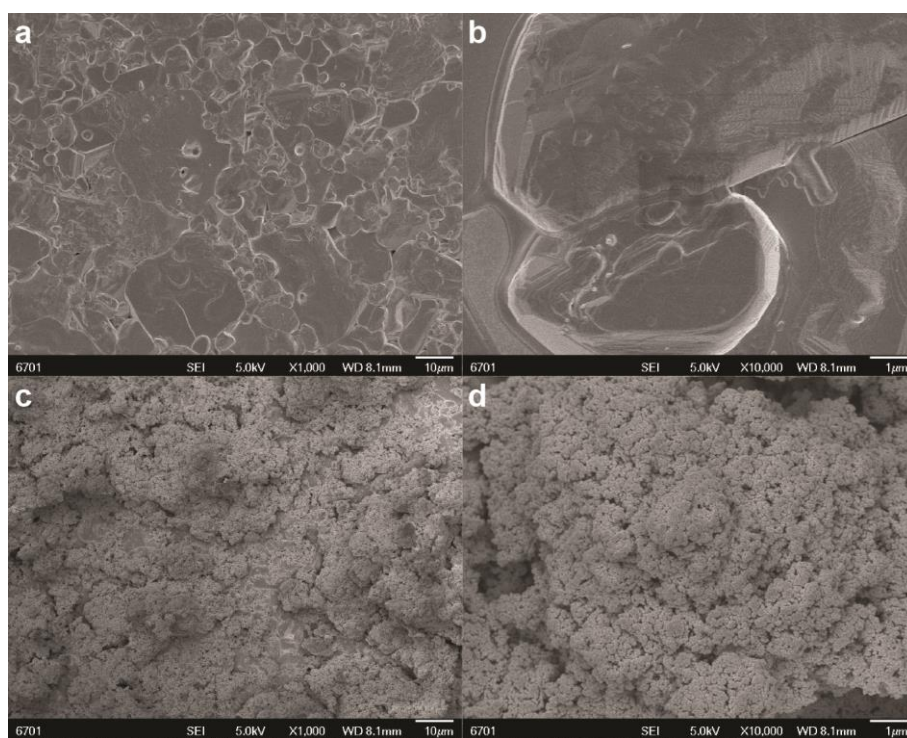


Fig. S19 SEM images of (a, b) original and (c, d) TiO₂-AP-FOTS coated ceramics.

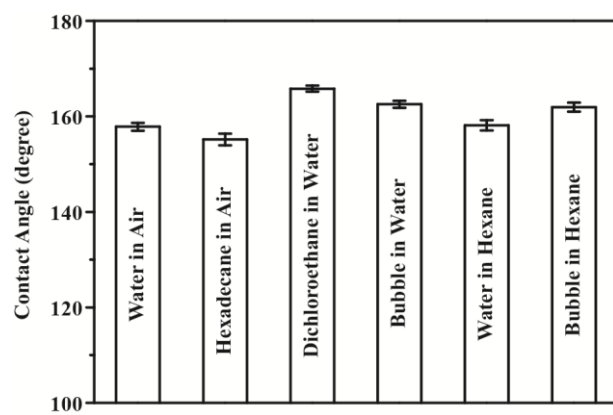


Fig. S20 Contact angles of the TiO₂-AP-FOTS coated ceramic for water in air, hexadecane in air, 1,2-dichloroethane under water, air bubble under water, water under hexane, and air bubble under hexane.

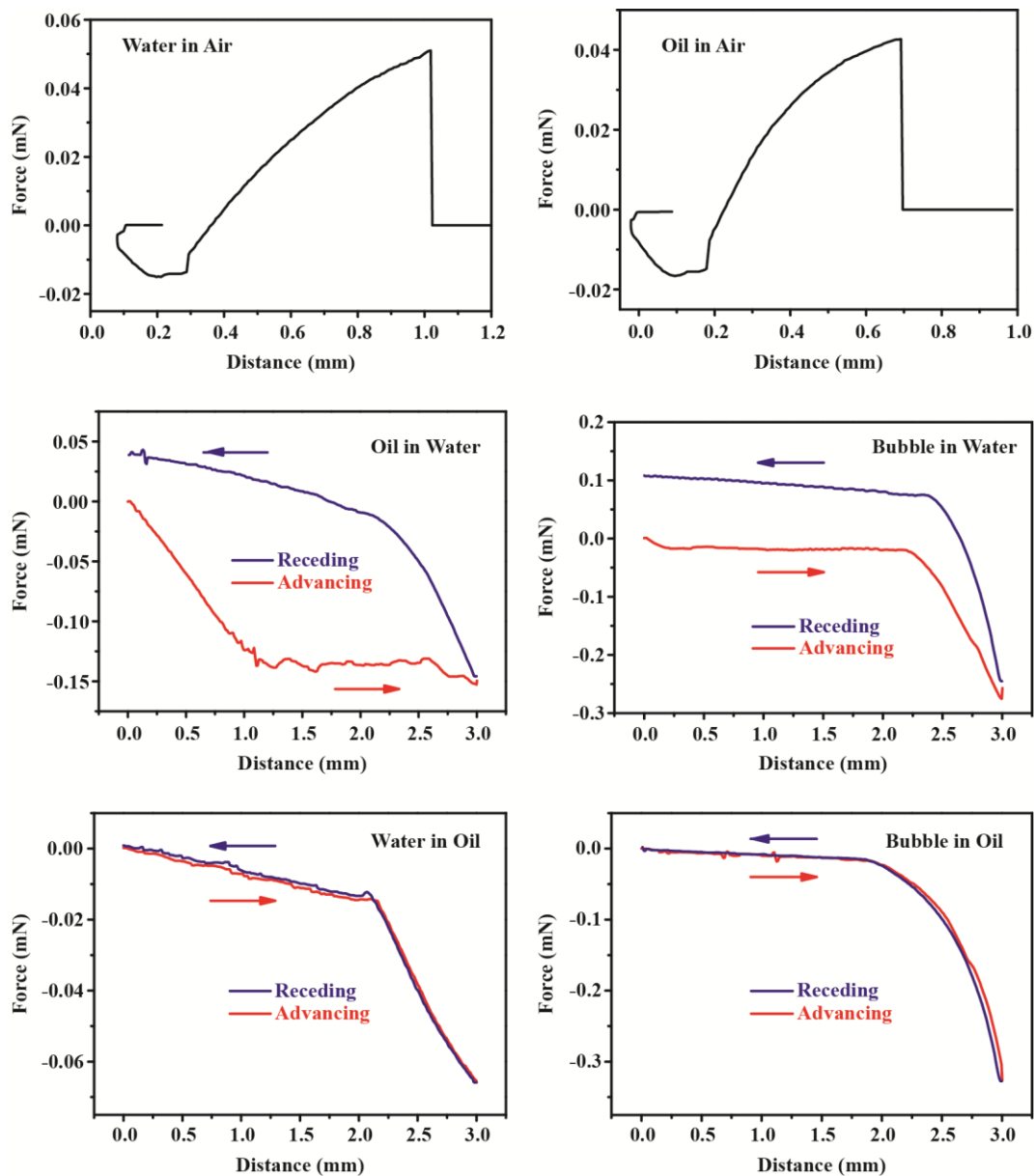


Fig. S21 Adhesion measurements of the TiO_2 -AP-FOTS coated ceramic: water in air, hexadecane in air, 1,2-dichloroethane under water, air bubble under water, water under hexane, and air bubble under hexane.

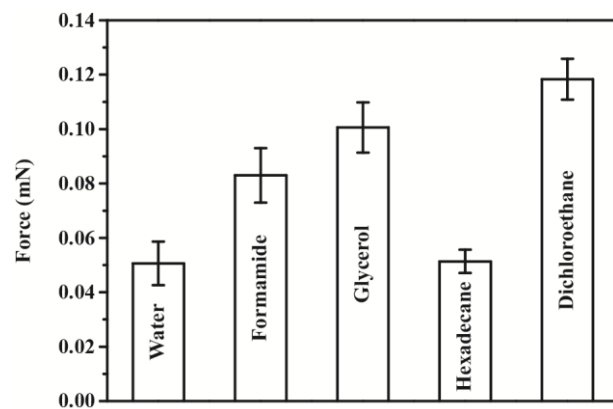


Fig. S22 Adhesive forces of water and oils deposited on the surface of the TiO₂-AP-FOTS coated ceramic.

Theoretical analysis

Young's equation

In the solid-water-air system:

$$\cos \theta_W = \frac{\gamma_{SA} - \gamma_{SW}}{\gamma_{WA}}$$

In the solid-oil-air system:

$$\cos \theta_O = \frac{\gamma_{SA} - \gamma_{SO}}{\gamma_{OA}}$$

In the solid-water-oil system:

$$\cos \theta_{W/O} = \frac{\gamma_{SO} - \gamma_{SW}}{\gamma_{OW}}$$

Combining the aforementioned Young's equations, $\theta_{W/O}$ is given as:

$$\cos \theta_{W/O} = \frac{\gamma_{WA} \cos \theta_W - \gamma_{OA} \cos \theta_O}{\gamma_{OW}}$$

and

$$\theta_{A/W} = 180 - \theta_W$$

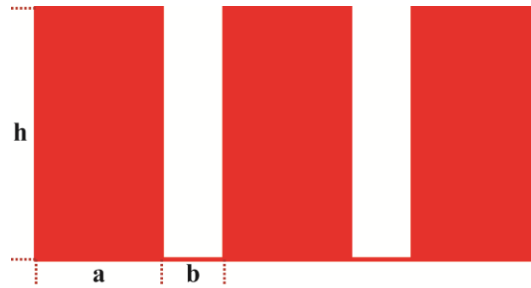
$$\theta_{A/O} = 180 - \theta_O$$

$$\theta_{O/W} = 180 - \theta_{W/O}$$

Cassie equation:

$$\cos \theta^* = f \cos \theta + f - 1$$

where θ and θ^* represent intrinsic and apparent contact angles for water (θ_W and $\theta_{W/A}^*$) and oil (θ_O and $\theta_{O/A}^*$) in air, underwater oil ($\theta_{O/W}$ and $\theta_{O/W}^*$) and air bubble ($\theta_{A/W}$ and $\theta_{A/W}^*$), and underoil water ($\theta_{W/O}$ and $\theta_{W/O}^*$) and air bubble ($\theta_{A/O}$ and $\theta_{A/O}^*$), respectively; γ stands for interfacial tensions; f is the area fraction.



$$f = \frac{a}{a + b}$$

Given f , the curves of the dependence of apparent contact angles (θ^*) including $\theta_{W/A}^*$, $\theta_{O/A}^*$, $\theta_{O/W}^*$, $\theta_{A/W}^*$, $\theta_{W/O}^*$, and $\theta_{A/O}^*$ on the surface chemistry (θ_W and θ_O) can be got.

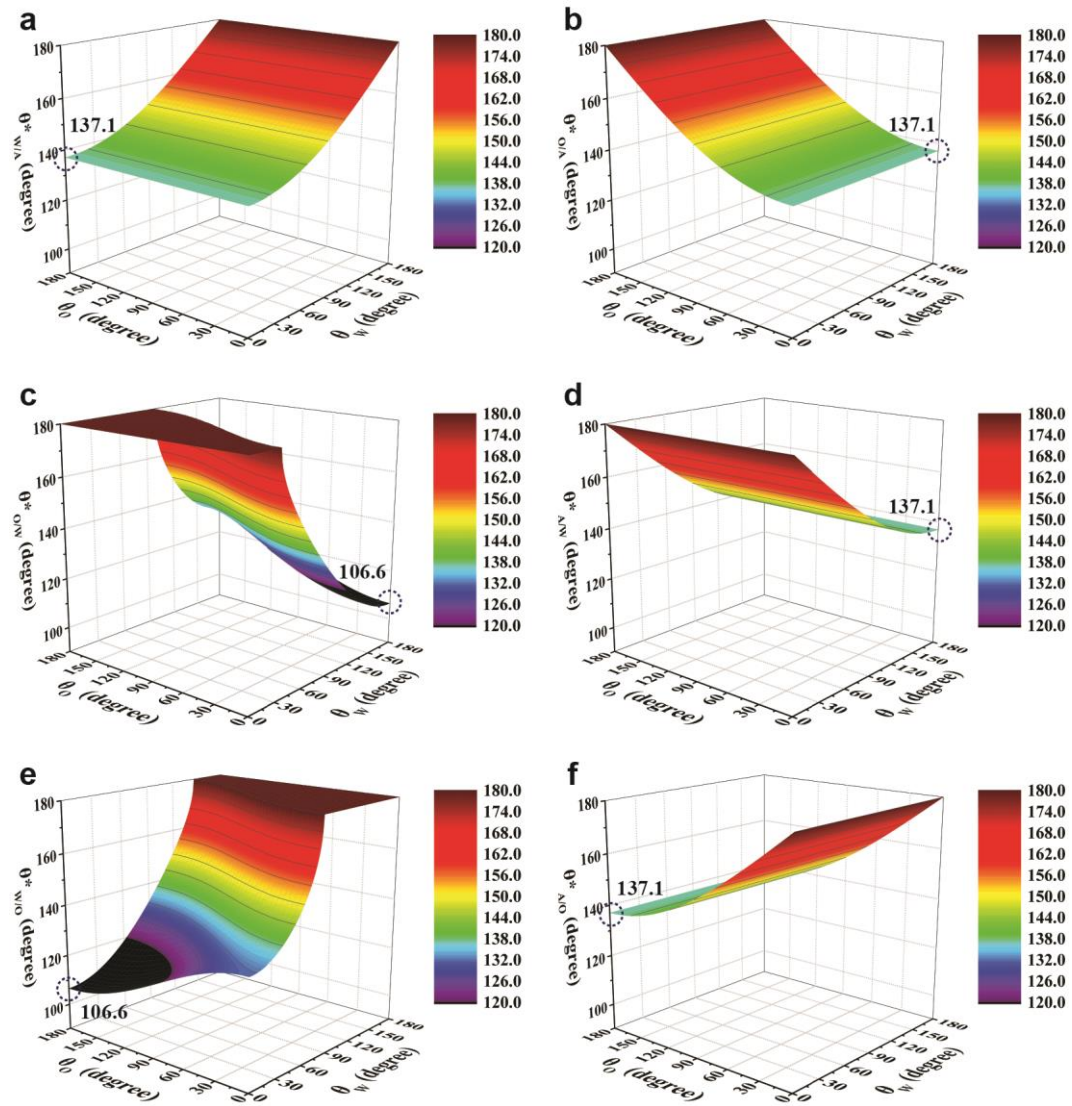


Fig. S23 The dependence of apparent contact angles (θ^*) including (a) $\theta_{W/A}^*$, (b) $\theta_{O/A}^*$, (c) $\theta_{O/W}^*$, (d) $\theta_{A/W}^*$, (e) $\theta_{W/O}^*$, and (f) $\theta_{A/O}^*$ on the surface chemistry (θ_w and θ_o) when f is 0.134.

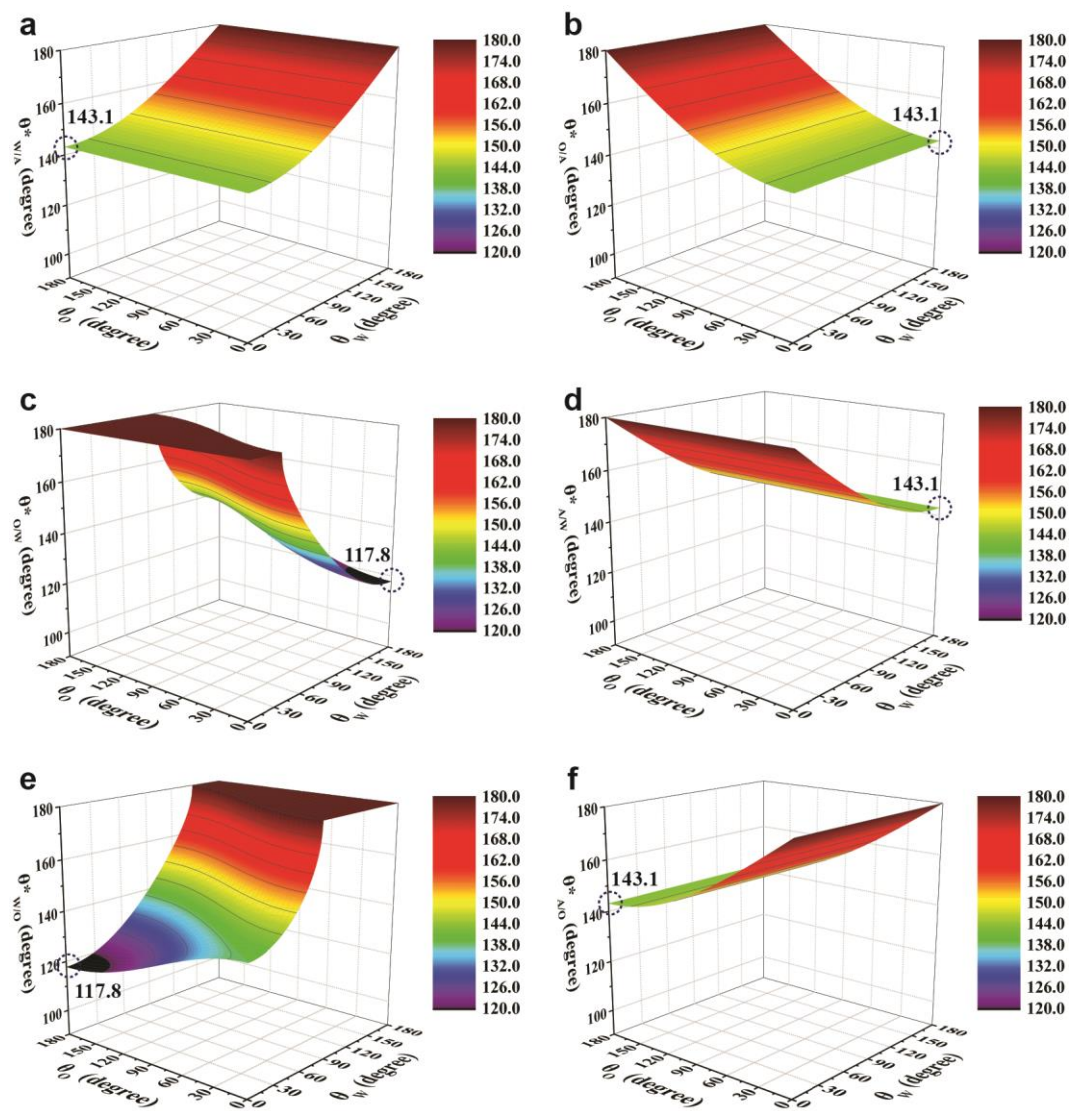


Fig. S24 The dependence of apparent contact angles (θ^*) including (a) $\theta_{w/A}^*$, (b) $\theta_{O/A}^*$, (c) $\theta_{O/W}^*$, (d) $\theta_{A/W}^*$, (e) $\theta_{W/O}^*$, and (f) $\theta_{A/O}^*$ on the surface chemistry (θ_w and θ_o) when f is 0.1.

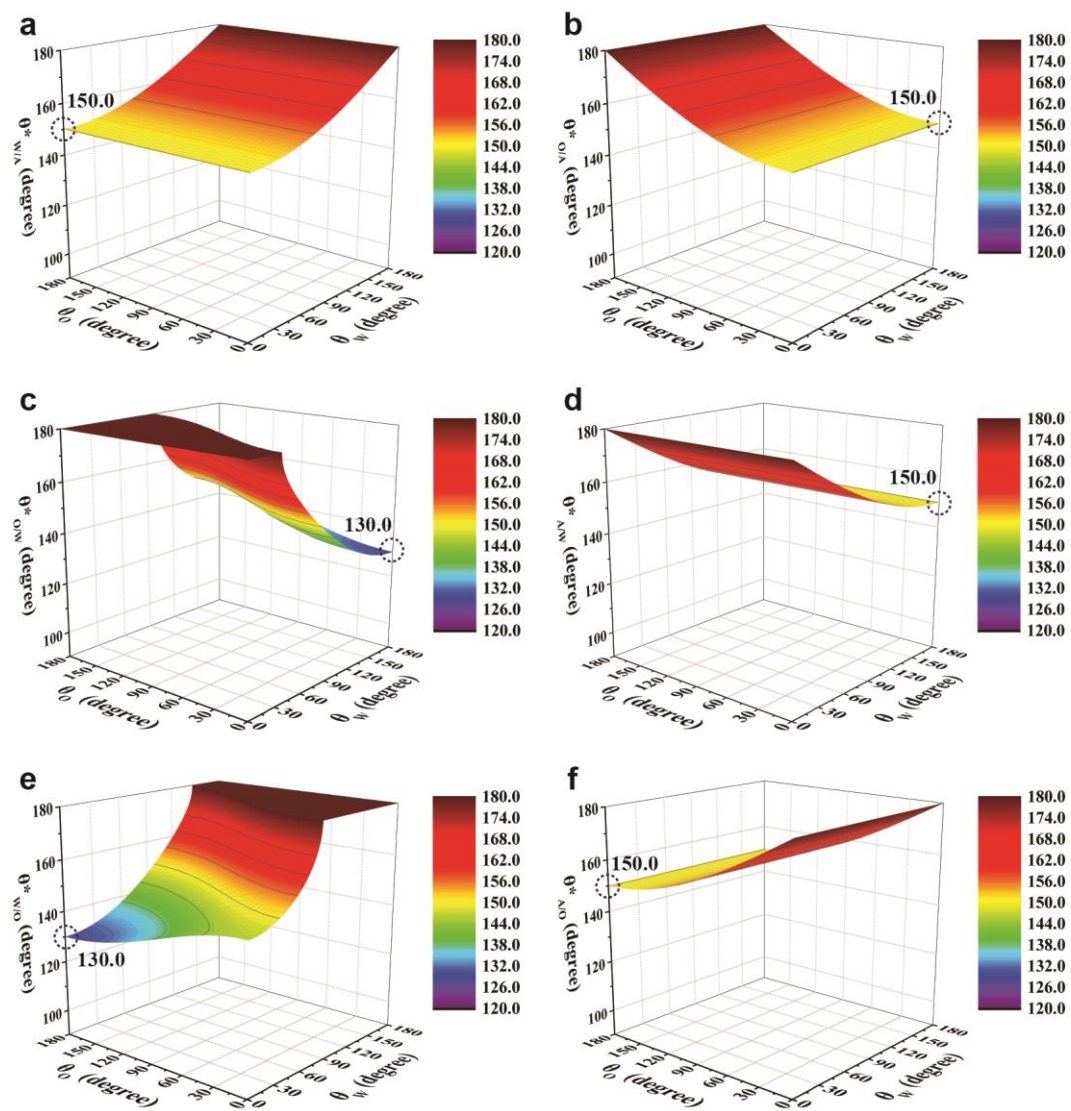


Fig. S25 The dependence of apparent contact angles (θ^*) including (a) $\theta_{W/A}^*$, (b) $\theta_{O/A}^*$, (c) $\theta_{O/W}^*$, (d) $\theta_{A/W}^*$, (e) $\theta_{W/O}^*$, and (f) $\theta_{A/O}^*$ on the surface chemistry (θ_w and θ_o) when f is 0.067.

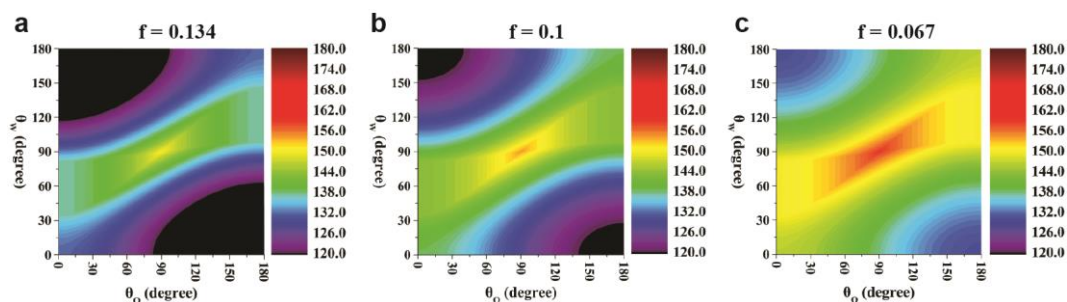


Fig. S26 Theoretical ranges of the surface chemistry (θ_w and θ_o) of all superantiwetting states: (a) $f = 0.134$, (b) $f = 0.1$, (c) $f = 0.067$.

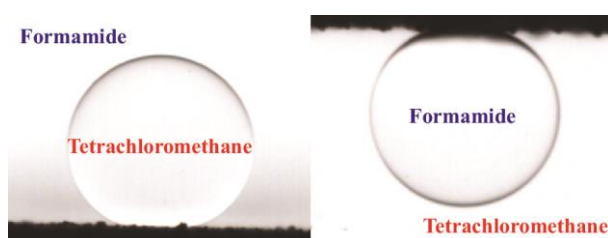


Fig. S27 Photographs of the TiO_2 -AP-FOTS coated SSM for CCl_4 under formamide and formamide under CCl_4 .

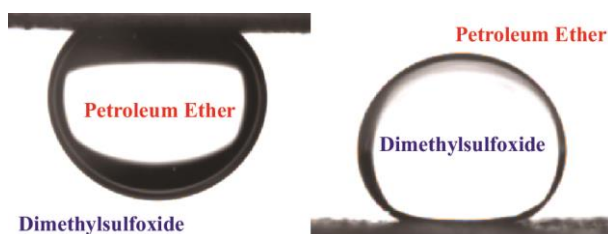


Fig. S28 Photographs of the TiO_2 -AP-FOTS coated SSM for petroleum ether under dimethylsulfoxide and dimethylsulfoxide under petroleum ether.

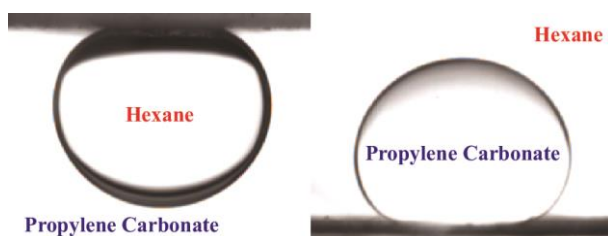


Fig. S29 Photographs of the TiO_2 -AP-FOTS coated SSM for hexane under propylene carbonate and propylene carbonate under hexane.

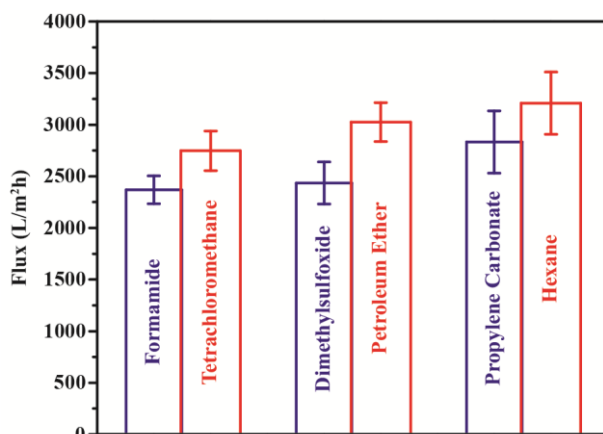


Fig. S30 Fluxes of the TiO₂-AP-FOTS coated SSM for separation of the immiscible organic liquids.

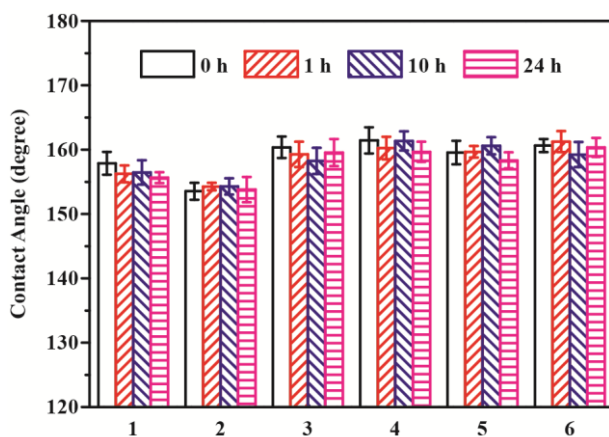


Fig. S31 Contact angles of the TiO₂-AP-FOTS coated SSM for water in air (1), hexadecane in air (2), 1,2-dichloroethane under water (3), air bubble under water (4), water under hexane (5), and air bubble under hexane (6) after UV irradiation for different time. The intensity and wavelength of UV light are 125 W and 365 nm, respectively. The distance between the TiO₂-AP-FOTS coated SSM and UV lamp is about 20 cm.

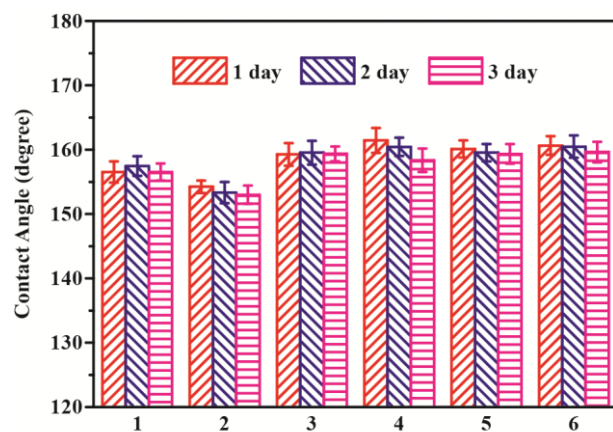


Fig. S32 Contact angles of the TiO₂-AP-FOTS coated SSM for water in air (1), hexadecane in air (2), 1,2-dichloroethane under water (3), air bubble under water (4), water under hexane (5), and air bubble under hexane (6) after immersion in water for different time.



Fig. S33 The process of the water impact test and SEM images of the TiO₂-AP-FOTS coated SSM after the water impact test for 10 cycles. Water droplets randomly impact the SSM surface and promptly bounce without any residual small water droplets.

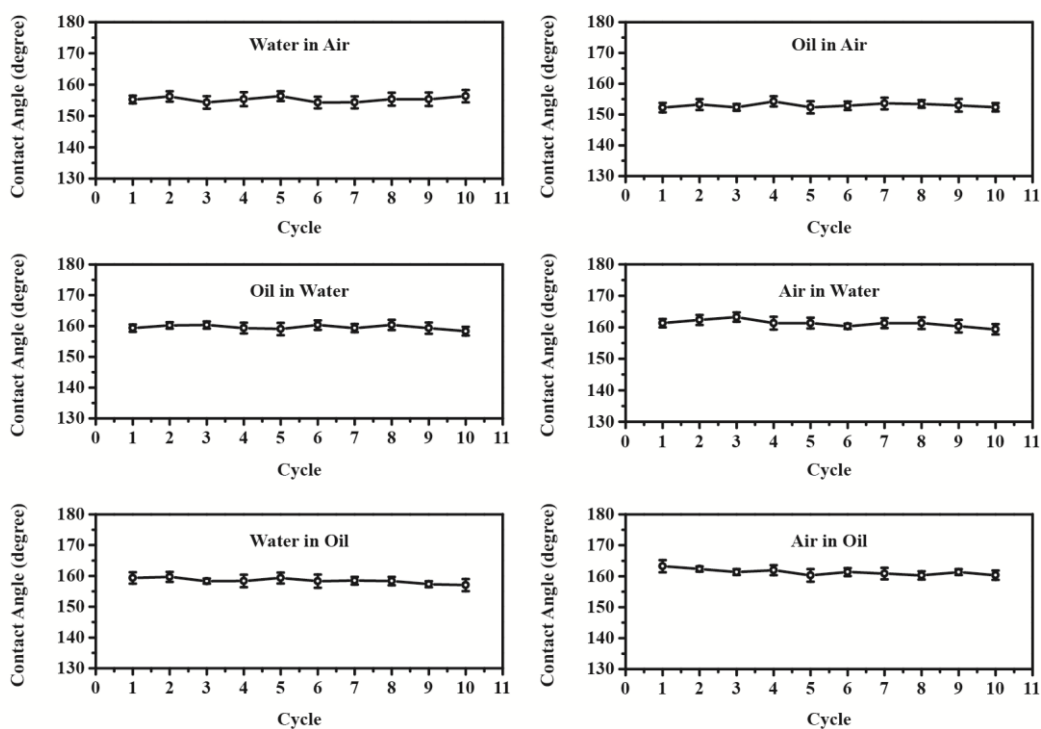


Fig. S34 Variation of the contact angles of the TiO_2 -AP-FOTS coated SSM for water in air, hexadecane in air, 1,2-dichloroethane under water, air bubble under water, water under hexane, and air bubble under hexane as a function of the number of cycles of the water impact test. One cycle uses 100 mL of water to rapidly and steadily impact the TiO_2 -AP-FOTS coated SSM using a washing bottle. After the water impact test for 10 cycles, the TiO_2 -AP-FOTS coated SSM maintains the all superantiwetting properties.

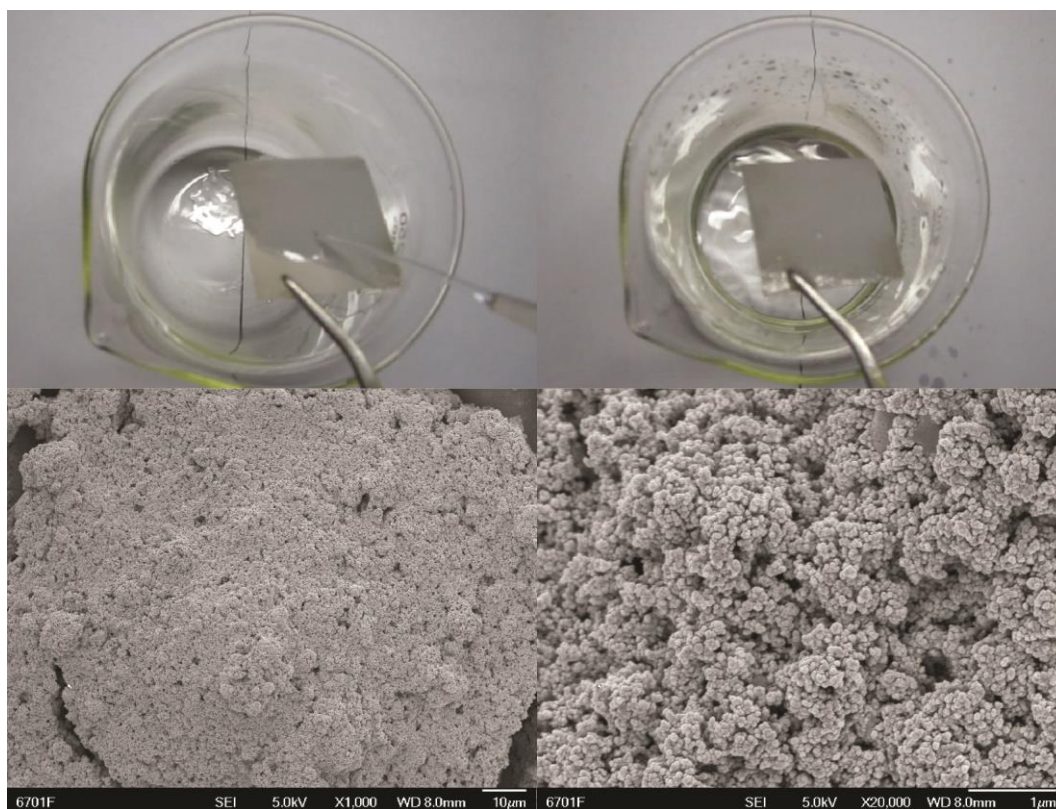


Fig. S35 The process of the ethanol impact test and SEM images of the TiO₂-AP-FOTS coated SSM after the ethanol impact test for 10 cycles. Ethanol easily wets and effectively impacts the SSM surface.

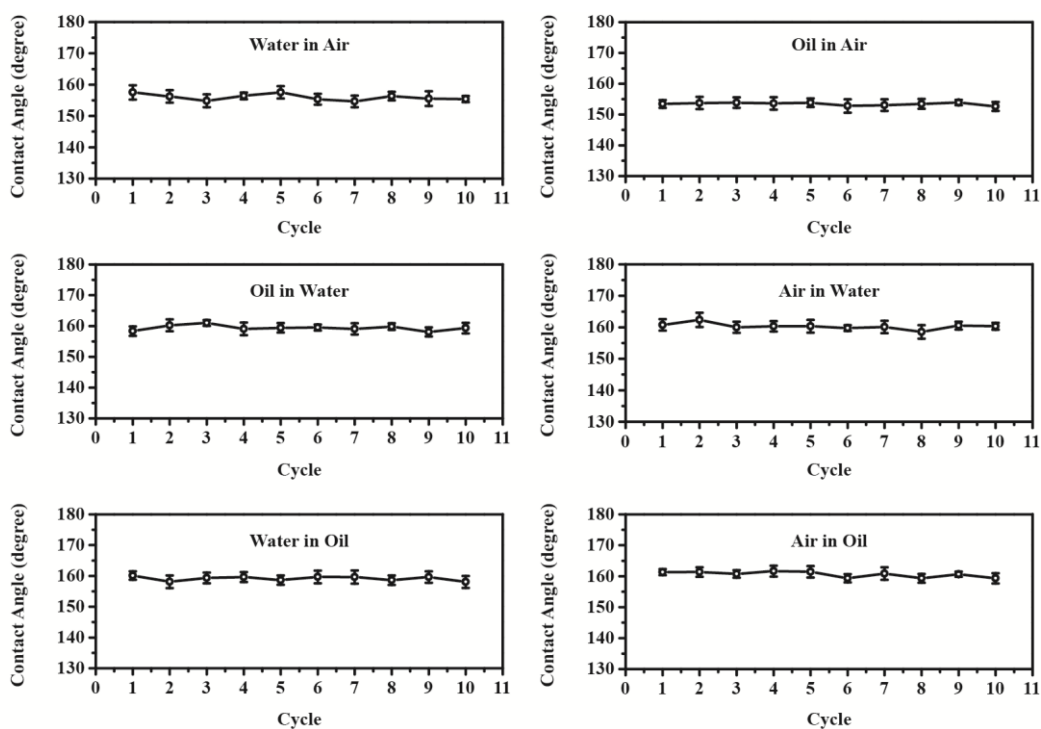


Fig. S36 Variation of the contact angles of the TiO_2 -AP-FOTS coated SSM for water in air, hexadecane in air, 1,2-dichloroethane under water, air bubble under water, water under hexane, and air bubble under hexane as a function of the number of cycles of the ethanol impact test. One cycle uses 100 mL of ethanol to rapidly and steadily impact the TiO_2 -AP-FOTS coated SSM using a washing bottle. After the ethanol impact test for 10 cycles, the TiO_2 -AP-FOTS coated SSM maintains the all superantiwetting properties.

Movie S1 The sliding processes for water in air, hexadecane in air, 1,2-dichloroethane under water, air bubble under water, water under hexane, and air bubble under hexane on the surface of the TiO₂-AP-FOTS coated SSM.

Movie S2 Separation of formamide-CCl₄ mixture by passing CCl₄ through the TiO₂-AP-FOTS coated SSM.

Movie S3 Separation of propylene carbonate-hexane mixture by passing propylene carbonate through the TiO₂-AP-FOTS coated SSM.

Movie S4 The process of the water impact test.

Movie S5 The process of the ethanol impact test.